Atmospheric mercury concentration and chemical speciation at a rural site in Beijing, China: implication of mercury emission sources

L. Zhang, S. X. Wang, L. Wang, and J. M. Hao

State Key Joint Laboratory of Environmental Simulation and Pollution Control, School of Environment, Tsinghua University, Beijing 100084, China

Correspondence to: S. X. Wang (shxwang@tsinghua.edu.cn)

Abstract. Continuous measurements of atmospheric mercury concentration and speciation play a key role in identifying mercury sources and its behavior in the atmosphere. In this study, speciated atmospheric mercury including gaseous elemental mercury (GEM), reactive gaseous mercury (RGM) and particle-bound mercury (PBM) were continuously measured at Miyun, a rural site in Beijing, China from December 2008 to November 2009. The average GEM, RGM and PBM concentrations were found to be 3.22±1.74 ng/m^3, 10.1±18.8 pg/m^3 and 98.2±112.7 pg/m^3, respectively, about 2–20 times of the background concentration of Northern Hemisphere. The results indicated that atmospheric mercury concentrations in North China were highly affected by anthropogenic emissions. The atmospheric mercury showed obvious seasonal variations with the highest seasonal average GEM concentration in summer (3.48 ng/m^3) and the lowest value in winter (2.66 ng/m^3). In autumn and winter a diurnal variation of GEM was observed with peak levels in late afternoon till midnight. Most of the high RGM concentration values occurred in the afternoon of all seasons due to the higher oxidation. The PBM concentration was higher in early morning of all seasons because of the atmospheric stratification during nighttime against laminar fluxes during daytime. The ratio of GEM to CO indicates that residential boilers play an important role in the elevation of GEM in winter. The ratio of RGM to O_3 could be an indicator of the contribution of local primary sources. The ratio of PBM to $PM_{2.5}$ reveals that the air mass from east and southwest to the site in spring and summer carries more atmospheric mercury. The HYSPLIT back-trajectory

analysis indicated that the monitoring site is affected by local, regional and interregional sources simultaneously during heavy pollution episodes. The results from the potential source contribution function (PSCF) model indicate that the atmospheric transport predominantly from the northwest contribute to the elevated atmospheric mercury in winter and autumn, while the North China Plain (NCP) Region and the north part of Yangtze River Delta (YRD) Region are the major source areas for mercury pollution in spring and summer.

1 Introduction

As a global pollutant, atmospheric mercury has been paid to great attention for its long-range transport and toxicity. Atmospheric mercury can be categorized into total gaseous mercury (TGM) and particle-bound mercury (PBM) in physical forms. TGM is further divided into gaseous elemental mercury (GEM) and reactive gaseous mercury (RGM). Schroeder and Munthe (1998) reported that GEM, accounting for over 95% of TGM, has a long residence time in the atmosphere from 0.5 to 2 years. However, based on soil–air exchange fluxes and deposition, Gustin et al. (2008) suggested that the residence time for GEM in the air is on the order of hours to weeks. Atmospheric mercury monitoring is a fundamental approach to understand the atmospheric mercury behavior of one region and is also used to identify the local and regional mercury emission sources coupling with back trajectory models.

According to the existing data, the global background concentration of atmospheric mercury is considered to be in the range of 1.5–1.7 ng/m^3 in the Northern Hemisphere and 1.1–1.3 ng/m^3 in the Southern Hemisphere (Fu et al., 2012a; Lindberg et al., 2007). There were plenty of studies conducted in the rural areas in the United States since 2000. Sheu et al. (2002) conducted a one-year study in Stillpond, Maryland and found the annual average GEM, RGM and PBM concentration to be 1.7±0.5 ng/m^3, 21±22 pg/m^3 and 42±50 pg/m^3, respectively. Studies conducted in Pompano Beach, Florida (Malcolm et al., 2003) showed similar results for GEM (1.6–2.0 ng/m^3) but much lower ranges for both RGM (1.6–4.9 pg/m^3) and PBM (0.7–6.3 pg/m^3). Lynam and Keeler (2005) reported that the GEM, RGM and PBM concentrations in Dexter, Michigan were respectively 1.49–1.51 ng/m^3, 2–3 pg/m^3 and 7–17 pg/m^3. Study of Gabriel et al. (2005) on Cove Mountain in Tennessee obtained a GEM average as high as 3.2 ng/m^3 and the RGM and PBM concentrations were 16.4 pg/m^3 and 9.7 pg/m^3, respectively. A five-year monitoring performed in Great Mountain Forest, Connecticut (Sigler and Lee, 2006) gave out a GEM range to be 1.4–1.6 ng/m^3. Similarly the GEM range of 1.3–1.6 ng/m^3 was found in Salmon Creek Falls Reservoir, Idaho (Abbott et al., 2007). Valente et al. (2007) reported the GEM, RGM and PBM concentrations to be 1.65 ng/m^3, 5 pg/m^3 and 7 pg/m^3 respectively in Look Rock, Tennessee. Laurier

and Mason (2007) found in Chesapeake Bay Laboratory, Maryland that the GEM and RGM concentrations were 1.7–1.8 ng/m^3 and 6–13 pg/m^3, respectively.

China is one of the largest mercury emission sources in the world (AMAP and UNEP, 2008). However, to date, relatively limited field measurements had been conducted in China to investigate the atmospheric processes of mercury. Most previous studies focused on the urban areas and mining/industrial regions (Fang et al., 2001; Liu et al., 2002; Feng et al., 2004; Wang et al., 2007; Zhu et al., 2012). A few studies were conducted at the mountain sites such as Mt. Waliguan, Mt. Gongga, and Mt. Changbai (Wang et al., 2007; Fu et al., 2008a, 2008b, 2009, 2010a; Zhu et al., 2008; Wan et al., 2009a, 2009b). There is lack of mercury monitoring data in rural area or regional background for typical regions in China such as North China Plain (NCP) Region. Most of these studies only measured atmospheric mercury and did not simultaneously observe the concentrations of other air pollutants such as fine particles ($PM_{2.5}$), carbon monoxide (CO), and ozone (O_3), which could help to identify the emission sources and explain the atmospheric behavior of mercury.

In this study, we measured the GEM, RGM and PBM as well as $PM_{2.5}$, CO, and O_3 at a rural site in North China for a whole year. We analyzed the temporal variation of mercury species and summarized the correlation between mercury and other air pollutants to investigate the factors affecting its behaviors in the region. Furthermore, based on the NOAA HYSPLIT model and the potential source contribution function (PSCF) model, the potential mercury sources and emission regions were analyzed, which helped to improve the understanding of atmospheric mercury outflow from China.

2 Methodology

2.1 Monitoring site description

The mercury monitoring station (40°28′51″ N, 116°46′30″ E, 220 m above sea level) in this study was located in Miyun County, about 100 km northeast to the Beijing urban area (see Fig. 1). The Miyun County is famous for its Miyun Reservoir, one of the biggest reservoirs in North China, supplying Beijing residents with fresh water.

The surrounding areas within 20 km from the site are largely rural, without large point source in any directions. Miyun has temperate continental monsoon climate, controlled by cold Siberian-Mongolian high pressure in winter with northwest wind dominated and impacted by Continental low and Pacific high pressure in summer with southeast wind dominated. The mercury emission sources in Beijing urban area are considered as the local sources for the monitoring station, which is shown in Fig. 1. The mercury emissions in the North China Plain (NCP) Region, including Beijing, Tianjin, Hebei, the north part of Henan and the west part of Shandong are regarded as regional sources for the site. The mercury emissions outside NCP region are all regarded as the interregional sources for this site.

2.2 Atmospheric mercury monitoring

Automatic atomic fluorescence mercury monitoring system, composed of Tekran^{TM} 2537B, 1130 and 1135, was employed in this study for measurements of GEM, RGM and PBM (Landis et al., 2002). Although Gustin et al. (2013) and Lyman et al. (2013) addressed that concentrations of reactive mercury (RGM+PBM) measured by the Tekran^{TM} system may be underestimated due to the release of mercury halides from KCl denuders in the presence of ozone, the Tekran^{TM} system is the most accurate instrument system so far and widely used for observation of speciated mercury in the ambient air.

The analytical module 2537B uses cold vapor atomic fluorescence spectroscopy (CVAFS) with the detection limit of 0.1 ng/m^3 (Landis et al., 2002) at the sampling flow rate of 1.0 L/min. GEM is continuously measured by 2537B every five minutes. The denuder coated with KCl in 1130 and the quartz filter in 1135 are designed to capture RGM and PBM respectively. Since there is an impactor at the bottom of 1130 to remove particles larger than 2.5 μm, PBM in this study is actually referred to $PBM_{2.5}$, i.e. the mercury on $PM_{2.5}$. The sampling inlet is 1.5 m above the instrument platform. Both units are configured to collect 1h samples at a flow rate of 10 L/min, resulting in a detection limit of 0.5 pg/m^3 for RGM and PBM (Landis et al., 2002). After 1h sampling, the quartz filter and the denuder turn to mercury desorption mode in succession at the temperature of 800°C and 500°C respectively. 1130 and 1135

systems are flushed with Hg-free air during the next 1h period, and RGM and PBM are sequentially thermodesorbed and analyzed. The denuder was recoated every two weeks in case of passivation. The 2537B analyzer was calibrated automatically every 25 h using the internal mercury permeation source inside the instrument, and the internal permeation source was calibrated every six months with manual injection of mercury by a syringe from an external mercury source (module 2505). Two zeros and two spans were performed in each calibration for gold trap A and B, respectively. The error between gold trap A and gold trap B was limited to ±10%. The impactor plate was changed once every two weeks. The quartz filter was changed once a month. The denuder was recoated once every two weeks following the procedure developed by Landis et al. (2002).

The meteorological parameters such as wind speed, wind direction, air temperature, and relative humidity were measured using Vantage Pro2^{TM} weather station (Davis Instruments). CO, O_3 and $PM_{2.5}$ concentrations were also monitored using Thermo Scientific^{TM} Model48i-TLE CO Analyzer, Model49i O_3 Analyzer and TEOM1405, respectively. The instrument details are discussed in Wang et al. (2008). All the data were hourly averaged for this study.

2.3 Meteorological data and backward trajectory calculation

The HYSPLIT (Hybrid Single-Particle Lagrangian Integrated Trajectory) model developed by the National Oceanic and Atmospheric Administration (NOAA) is a complete system for computing simple air parcel trajectories to complex dispersion and deposition simulations. In this study, Global Data Assimilation System (GDAS) data with one-degree latitude-longitude horizontal resolution was used for source identification. Back trajectories were calculated for typical pollution events. The total run time was 48 h which can cover China, Mongolia and east Russia. The start time was 4:00 am (UTC) and restarted every 6 hours. The trajectory arrival height (a.g.l) was set as 500 m above surface ground to represent the boundary layer where pollutants are usually well mixed.

The potential source contribution function (PSCF) is a useful statistical tool based on the HYSPLIT model to identify source areas for pollutants with a relatively long

life-time such as elemental mercury and CO (Xu and Akhtar, 2010). The PSCF values for mean GEM concentrations in grid cells in a study domain are calculated by counting the trajectory segment endpoints that terminate within each cell. The number of endpoints that fall in the *ij*th cell is designated n_{ij}. The number of endpoints for the same cell having arrival times at the sampling site corresponding to GEM concentrations higher than a specific criterion is defined to be m_{ij}. The PSCF value for the *ij*th cell is then defined as:

$$\mathrm{PSCF}_{ij} = \frac{m_{ij}}{n_{ij}} W_{ij} \quad (1)$$

Where W_{ij} is an empirical weight to reduce the effects of grid cells with small n_{ij} values. In this study, W_{ij} is defined in following formula in which *Avg* is the mean n_{ij} of all grid cells with n_{ij} greater than zero.

$$W_{ij} = \begin{cases} 1.0 & n_{ij} > 2 \cdot Avg \\ 0.7 & Avg < n_{ij} \le 2 \cdot Avg \\ 0.42 & 0.5 \cdot Avg < n_{ij} \le Avg \\ 0.17 & n_{ij} \le 0.5 \cdot Avg \end{cases} \quad (2)$$

The PSCF value indicates the probability of a grid cell through which pollution events occurs. More details can be found in the study of Polissar et al. (1999). In this study, the domain which covers Chinese mainland (73.5° E – 134.5° E, 18.5° N – 53.5° N), is divided into 8450 grid cells with 0.5° × 0.5° resolution. Three-day back trajectories are generated hourly from January 1 to November 11 in 2009 by TrajStat (Wang et al., 2009), a software including HYSPLIT for trajectory calculation with trajectory statistics modules. PSCF maps are plotted using ARCGIS version 9.3.

3 Characteristics of Speciated Mercury Concentration

3.1 General characteristics of speciated mercury in atmosphere

Speciated mercury concentration data with a one-year period from December 2008 to November 2009 was obtained by the Tekran™ mercury monitoring system. The hourly averaged GEM, RGM and PBM concentrations are shown in Fig. 2. The average GEM concentration in Miyun Station is 3.22±1.74 ng/m^3, while those of

185 RGM and PBM are 10.1±18.8 pg/m^3 and 98.2±112.7 pg/m^3, respectively (see Table 1).
186 GEM accounts for over 95% of the total mercury concentration. The average total
187 mercury concentration is 3.3 ng/m^3, about 2 times of the background concentration of
188 Northern Hemisphere (Lindberg et al., 2007). The median value of GEM is 9% lower
189 than the mean value. The interval of 1st and 3rd quartiles lies in the range of 1.81–4.12
190 ng/m^3. However, the mean values of RGM and PBM are much higher than the median
191 values respectively. The mean/median ratios for RGM and PBM are 2.0 and 1.7,
192 respectively. Comparing the mean values of RGM and PBM with the results from the
193 monitoring sites in rural areas in the USA (Valente et al., 2007; Gabriel et al., 2005;
194 Lynam and Keeler, 2005; Malcolm et al., 2003), the RGM concentration of the Miyun
195 site is more or less at the same level as those of American sites. However, the PBM
196 concentration of the Miyun site is much higher than those of American sites, which
197 reflects the severe PM pollution problem in North China. Table 2 listed the TGM,
198 PBM and RGM concentrations of mercury monitoring sites in China from existing
199 literatures. The TGM concentration of this rural site in Beijing is higher than that of
200 most remote sites, while lower than that of most urban sites. The PBM concentration
201 of this rural site in Beijing is higher than that of all remote sites, while lower than that
202 of all urban sites. The PBM/GEM ratio at Miyun site is higher than most of the
203 monitoring sites in China except Guiyang urban site, while the RGM/GEM ratio at
204 this site is lower than most of the sites in China except Mt. Gongga site (see Table 2).
205 This is probably a characteristic of atmospheric mercury in North China due to the
206 heavy PM pollution. There are several extreme peaks in the observation of the three
207 mercury species. Most of the GEM and PBM peaks match well with the highest air
208 pollution index (API) values in Beijing urban area (shown in Fig. 2), indicating the
209 influence of heavy pollution episodes in Beijing, especially for the period of
210 November 3rd to 8th, 2009. It should be noted that PM_{10} is the dominant pollutant for
211 Beijing's API in heavy pollution episodes.

212 **3.2 Seasonal variation of speciated mercury concentration**

213 The monthly variation of GEM and the seasonal variation of RGM and PBM are
214 shown in Fig. 3. December–February is considered to be winter, March–May to be

spring, June–August to be summer, and September–November to be autumn. The highest seasonal average GEM concentration occurs in summer (3.48 ng/m^3), while winter has the lowest value (2.66 ng/m^3). This is probably due to the long-range transport related to the dominant wind direction, which will be discussed in detail in Section 5.2. The dominant wind direction for spring, summer and autumn was southwest, while the wind was mainly from north and northwest in winter. However, the case of PBM concentration is the opposite. The PBM concentration is higher in winter and lower in summer. The variation range of GEM is relatively larger in spring and autumn than that in winter and summer. The variation range of PBM is smaller in summer than other seasons. From winter to autumn, the RGM concentration gets higher, and the variation range of it becomes larger. RGM is either directly released by anthropogenic sources or formed by the photochemical processes with the oxidation of GEM. The seasonal variation of RGM indicates that the photochemical oxidation processes were more active in summer and autumn than in winter and spring. The heavy pollution episodes in autumn were longer and heavier than those in other seasons due to the disadvantageous diffusion condition, which led to the highest seasonal average RGM concentration in autumn.

3.3 Diurnal variation of speciated mercury concentration

The overall daytime average concentrations of GEM, RGM and PBM were 3.13 ng/m^3, 11.5 pg/m^3 and 83.6 pg/m^3, respectively, while the overall nighttime averages of the three species were 3.30 ng/m^3, 8.7 pg/m^3 and 112.0 pg/m^3, respectively. In spring and summer, no significant diurnal variation is found for GEM, as is shown in Fig. 4a. The GEM concentration from late afternoon till midnight (16:00 – 2:00) is higher than the rest of the day in autumn and winter. For the RGM concentration in Fig. 4b, most of the high values occur in the afternoon (13:00 – 15:00) of all four seasons. This is probably related to the intensity of solar radiation. With higher intensity of solar radiation in the afternoon, more GEM is oxidized to RGM. However, the RGM concentration peak for autumn is higher than that for summer, which is due to the disadvantageous diffusion condition in autumn. The PBM concentration, shown in Fig. 4c, is higher in the early morning (1:00 – 6:00) of all four seasons, which is

probably caused by atmospheric stratification during nighttime against laminar fluxes during daytime, driven by wind secular periodicity. The daily variation of RGM and PBM reflects the formation and removal mechanisms of these two short lifetime mercury species. Photochemical reaction is the main process for RGM formation, while deposition and adsorption to particles are the two main processes for RGM removal. Adsorption of GEM and RGM to particles is the main process for PBM formation, while rain and dispersion are important processes for PBM removal.

3.4 Correlations between mercury species and meteorological factors

Among all meteorological factors, wind direction has the most significant impact on the concentrations of different mercury species. Fig. 5 shows the GEM, RGM and PBM concentrations and wind direction frequency in different wind directions. Southwest wind was the dominant wind direction in the monitoring period with both high frequency and high wind speed. The high average GEM and PBM concentrations from the southwest direction suggest that the southwest wind brought the most atmospheric mercury pollution to the monitoring site. The influence of wind direction on RGM is not as remarkable as that on GEM and PBM, because RGM is also highly related to other meteorological factors, such as solar radiation. Temperature and relative humidity also has considerable influence on different mercury species with seasonal variations, as shown in Table 3. RGM concentration has higher dependence on temperature in spring and summer than in autumn and winter, indicating higher RGM formation from photochemical reactions in spring and summer. No correlation was found between temperature and GEM or PBM concentration. The correlations between GEM concentration and relative humidity are notable with little seasonal variation, which is possibly due to the same pattern of diurnal variation of GEM and relative humidity, i.e. lower at daytime and higher at night. RGM concentration is positively related to relative humidity in winter while negatively in summer. It reveals that moisture in the atmosphere could both scavenge RGM by wet deposition under higher temperature in summer and enhance RGM formation by strengthening the oxidation process under lower temperature in winter. PBM concentration has considerable correlation with relative humidity, higher in winter than other seasons.

This implies that moisture probably contributes to the formation of PBM, and this influence is amplified under lower temperature.

4 Mercury Source Attribution via Multi-Pollutant Correlations

4.1 Source type identification

GEM concentration has a significant correlation with CO concentration due to their homology. Industrial coal combustion, domestic coal combustion, cement production and iron and steel production are the dominant anthropogenic emission sources for both pollutants (Wu et al., 2006; Wang et al., 2005). Except for these four types of sources, vehicles are another type of dominant sources for CO, while power plants and non-ferrous metal smelters are another two types of dominant sources for GEM. GEM also has significant natural background, which CO does not. Fig. 6 shows the relationship between GEM concentration and CO concentration by season.

The slope of the trend line represents the ratio of GEM emission to CO emission (Hg/CO ratio). For the monitoring station in this study in North China, the GEM concentration is mainly influenced by coal combustion, including power plants, industrial boilers and residential boilers, while the CO concentration is mainly influenced by coal combustion and vehicles. Non-ferrous metal smelters, the second largest anthropogenic source of mercury, are mainly located in the southern part of China, and thus have little influence on the GEM concentration of this station. Based on existing studies (Wang et al., 2005; Wu et al., 2006), the Hg/CO ratio for power plants is larger than that for industrial and residential boilers. In 2001, the Hg/CO ratios for power plants, industrial boilers and residential boilers were 25.2, 2.9 and 0.4, respectively (Wang et al., 2005; Wu et al., 2006). Incomplete combustion such as residential coal combustion and biomass burning could lead to a lower Hg/CO ratio. The Hg/CO ratio for vehicles is almost zero. Weiss-Penzias et al. (2007) reported Hg/CO ratios of 5.7, 1.5 and 0.8 for Asian long-range transport (ALRT), Pacific Northwest U.S. biomass burning (BB PNW) and Alaska biomass burning (BB Alaska), respectively. As shown in Fig. 6, The Hg/CO ratio for winter, spring, summer and autumn are 1.50, 3.04, 2.43 and 3.24, respectively. One of the main causes for the

lower Hg/CO ratio in winter could be that the activity level of residential coal combustion is higher in winter. The Hg/CO ratios in Fig. 6 indicate that residential boilers play an important role in mercury pollution in winter.

The intercept of the trend line mainly reflects the intensity of natural background of GEM. The intercept for summer is higher than those for other seasons because the natural mercury emissions are higher in summer in terms of higher atmospheric temperature. However, the intercept for autumn is lower than that for winter, which is probably due to the heavy GEM pollution episodes. Most of the GEM concentration values higher than 10 ng/m^3 were from November 5th and 6th, 2009, resulting in the counterclockwise rotation of the trend line and thus the decrease of the intercept.

The correlation coefficients of the trend lines for winter, spring, summer and autumn are 0.89, 0.71, 0.74 and 0.79 respectively. The correlation coefficient implies the contribution rate of homological emission sources (e.g. industrial coal combustion, residential coal combustion, cement production and iron and steel production) to GEM concentration, which fits quite well with the fact that the correlation coefficient for winter is much higher than that for other seasons, because the activity level of coal combustion in North China is higher in winter for heating supply.

4.2 Impacts of local primary sources

O_3 is a secondary pollutant and originates from photochemical process and thus highly depends on the intensity of solar radiation. RGM is formed either directly from local emission sources (i.e. primary RGM) or from the photochemical oxidation of GEM (i.e. secondary RGM). Considering the shorter residence time of both RGM and O_3 compared with GEM, the primary RGM emitted directly from emission sources can be considered as the direct influence of the local sources.

The comparison of O_3 and RGM concentrations in different seasons is shown in Fig. 7. In winter, both the RGM and O_3 were at low level due to low intensity of radiation, while both concentrations were high in summer. The coherence of the variation of RGM and O_3 was high in spring and summer while low in autumn and winter. This indicates that the monitoring site is more directly influenced by local sources in autumn and winter, while the secondary RGM is more important in spring and

summer.

After sequencing the RGM/O_3 ratio, the moving correlation coefficients of every 100 pairs of O_3-RGM were calculated. Fig. 8 shows the relationship between the moving average RGM/O_3 ratio and the moving O_3-RGM correlation coefficient. It reveals that the O_3-RGM correlation coefficient decreases when the RGM/O_3 ratio increases in the range of 0.05–2 $pg \cdot m^{-3} \cdot ppb^{-1}$. This implies that the ratio of RGM to O_3 could be an indicator of local primary sources. Higher RGM/O_3 ratio suggests higher influence from local primary sources. The exceptions outside the common RGM/O_3 ratio range were mainly because the RGM or O_3 concentrations were fairly low (RGM < 1 $pg \cdot m^{-3}$, O_3 < 2 ppb). The peak values of the RGM/O_3 ratio occurred in the period from November 3rd to 8th, 2009. The back trajectory analysis indicated that this period was mainly influenced by local emission sources, as shown in Section 5.1.

4.3 Source direction identification

Relationships between PBM and $PM_{2.5}$ have obvious seasonal variations, as shown in Fig. 9. The slope of the trend line means the ratio of PBM to $PM_{2.5}$. The ratios for winter, spring, summer and autumn are 2.66×10^{-6}, 3.06×10^{-6}, 3.35×10^{-6} and 2.56×10^{-6}, respectively. Wind direction is a key factor for the variations. Based on the meteorological data, the dominant wind directions for all the four seasons are northeast wind. However, the subdominant wind direction for spring and summer are east wind and southwest wind. The particles from the north are mainly sand storms from Inner Mongolia, a natural source of particles whose mercury content is low. The particles from the south are mainly from North China Region including Beijing urban area. Most of these particles with high mercury content are emitted from anthropogenic sources, such as coal-fired boilers. Therefore, the slope of the trend line for the relationship between $PM_{2.5}$ and PBM could reveal the mercury source direction. The ratios reveal that the air mass from east and southwest to the site in spring and summer carries more atmospheric mercury.

5 Mercury Source Attribution via HYSPLIT Modeling

5.1 Identification of mercury sources during heavy pollution episodes

HYSPLIT is a modeling tool to visualize the long-range transport of air mass so as to track the spatial sources of certain pollutants. HYSPLIT modeling was performed for three heavy pollution episodes respectively in spring, summer and autumn, May 4^{th}–6^{th} (episode I), August 12^{th}–14^{th} (episode II) and November 5^{th}–7^{th} (episode III), 2009 with a runtime of 48 hours, shown as Fig. 10. The average GEM, RGM and PBM concentrations for these three episodes are listed in Table 1. The dominant mercury species for the first episode in spring were GEM and PBM, while that for the second episode in summer was RGM. The concentrations of all the three mercury species were significantly high for the third episode in autumn. The air mass in the spring case in the period of May 4^{th}–6^{th} was transported from Yangtze River Delta (YRD) Region to North China Plain (NCP) Region. Almost all the air mass came from low atmospheric level with heavy polluted air mass. This is a typical pollution period in spring. The air mass transport in the summer case in the period of August 12^{th}–14^{th} was within shorter distance than that in the spring case. The air mass in this period was mainly from Southwest China to North China. The air mass in the period of November 5^{th}–7^{th} was mainly from the Northwest China to North China. The air mass traveled from the remote northwestern area where the air was relatively clean to the Loess Plateau (including part of Gansu, Ningxia, Shanxi and Shaanxi Province), descending from high altitude to low altitude. The air originated from the Loess Plateau was mainly at low atmospheric level and carried with polluted air from urban area. The three heavy pollution episodes indicate that the monitoring site is affected by local, regional and interregional sources simultaneously. Both the HYSPLIT results and the RGM/O_3 ratios suggest that the mercury pollution in episode I is more impacted by the interregional sources in YRD Region, the episode II is more impacted by the regional sources in NCP Region, and the episode III is more impacted by the local sources.

5.2 Spatial distribution of mercury emission sources by PSCF statistics

Influence of the regional or interregional sources can be identified by the PSCF model with the year-round statistics. Fig. 11a shows the overall spatial contribution of mercury emission sources in East Asia. NCP Region, mainly the part to the south of

Beijing, might have significant impacts on the atmospheric mercury distribution pattern at the Miyun monitoring site. The contribution for each season is also given in Fig. 11. In winter and autumn, most of the mercury comes from the remote west and north area, including the Loess Plateau and Outer Mongolia. On the contrary, the major sources of mercury in spring and summer are located in the south and east area to Beijing. In summer, NCP Region, especially Shandong and Hebei provinces, are the two major contributors. In spring, the contributing area expands to Henan, Anhui and Jiangsu, which has reached the north of YRD Region. The year-round statistics indicate that mercury emission in NCP is the most important contributor of mercury pollution in Miyun site. However, it has to be noted that HYSPLIT model has its limitation and the results could be interfered by the "local signal".

6 Conclusions

The one-year speciated mercury observation in Miyun from December 2008 to November 2009 indicated that the overall average GEM, RGM and PBM concentrations are 3.22±1.74 ng/m^3, 10.1±18.8 pg/m^3 and 98.2±112.7 pg/m^3, respectively. The seasonal average GEM concentration is higher in summer and lower in winter. The PBM concentration, on the contrary, is higher in winter and lower in summer. RGM, formed by the photochemical processes, has higher concentration and wider range in autumn. No significant daily variation is found for GEM in spring and summer, while in autumn and winter the GEM concentration from late afternoon till midnight is higher than the rest of the day. Most of the high RGM concentration values occur in the afternoon due to the high intensity of solar radiation. The PBM concentration is higher in the early morning of all four seasons, which is probably related to atmospheric stratification during nighttime against laminar fluxes during daytime, driven by wind secular periodicity.

GEM concentration has a significant correlation with CO concentration due to their homology. The slope of the trend line represents the ratio of GEM emission to CO emission, which indicates that residential boilers play an important role in the mercury pollution in winter. The intercept of the trend line reflects the intensity of

natural background of GEM. The correlation coefficient of GEM and the CO concentration implies the contribution rate of coal combustion to GEM. The ratio of RGM to O_3 could be an indicator of local primary sources. Moreover, the ratio of PBM to $PM_{2.5}$ indicates that the air mass from east and southwest to the site in spring and summer carries more atmospheric mercury.

From the analysis of heavy pollution episodes using the HYSPLIT model, the monitoring site is simultaneously affected by local, regional and interregional sources, and the most heavily polluted episode is more impacted by the local sources. According to the PSCF statistics based on HYSPLIT model, most of the mercury comes from the remote west and north area to Beijing, including the Loess Plateau and Outer Mongolia in autumn and winter. However, the major sources of mercury in spring and summer are located in the south and east area to Beijing. Mercury emissions from NCP Region to the north part of YRD Region play a more important role in spring and summer than that in autumn and winter.

Acknowledgment. This work was sponsored by Natural Science Foundation of China (No. 20 937002), Major State Basic Research Development Program of China (973 Program) (No. 2013CB430001) and MEP's Special Funds for Research on Public Welfares (No. 201209015). We would like to thank Dr. Nicola Pirrone for his help on the establishment of Miyun mercury monitoring station and Dr. Jerry Lin for his valuable suggestions on this paper.

References

Abbott, M., Lin, C.J., Martian, P., and Einerson, J.: Atmospheric Mercury Near Salmon Falls Creek Reservoir in Southern Idaho, INL/EXT-06-12048, Idaho Department of Environmental Quality, Boise, Idaho, 2007.

Arctic Monitoring and Assessment Programme (AMAP), and United Nations Environment Programme (UNEP): Technical Background Report to the Global Atmospheric Mercury Assessment, Geneva, Switzerland, 2008.

Ci, Z. J., Zhang, X. S., Wang, Z. W., and Niu, Z. C.: Atmospheric gaseous elemental mercury (GEM) over a coastal/rural site downwind of East China: temporal variation and long-range transport, Atmos. Environ., 45, 2480–2487, 2011a.

Ci, Z. J., Zhang, X. S., Wang, Z. W., Niu, Z. C., Diao, X. Y., and Wang, S. W.: Distribution and air-sea exchange of mercury (Hg) in the Yellow Sea, Atmos. Chem. Phys., 11, 2881–2892, 2011b.

Fang, F. M., Wang, Q. C., Liu, R. H., Ma, Z. W., and Hao, Q. J.: Atmospheric particulate mercury in Changchun City, China, Atmos. Environ., 35, 4265–4272, 2001.

Fang, F. M., Wang, Q. C., and Li, J. F.: Urban environmental mercury in Changchun, a metropolitan city in Northeastern China: source, cycle, and fate, Sci. Total. Environ., 330, 159–170, 2004.

Feng, X. B., Shang, L. H., Wang, S. F., Tang, S. L., and Zheng, W.: Temporal variation of total gaseous mercury in the air of Guiyang, China, J. Geophys. Res., 109, 3303, 2004.

Friedli, H. R., Arellano, A. F., Geng, F., Cai, C., and Pan, L.: Measurements of atmospheric mercury in Shanghai during September 2009, Atmos. Chem. Phys., 11, 3781–3788, 2011.

Fu, X. W., Feng, X. B., Zhu, W. Z., Wang, S. F., and Lu, J. L.: Total gaseous mercury concentrations in ambient air in the eastern slope of Mt. Gongga, South-Eastern fringe of the Tibetan plateau, China, Atmos. Environ., 42, 970–979, 2008a.

Fu, X. W., Feng, X. B., Zhu, W. Z., Zheng, W., Wang, S. F., and Lu, J. Y.: Total particulate and reactive gaseous mercury in ambient air on the eastern slope of the Mt. Gongga area, China, Appl. Geochem., 23, 408–418, 2008b.

Fu, X. W., Feng, X. B., Wang, S. F., Rothenberg, S., Shang, L. H., Li, Z. G., and Qiu, G. L.: Temporal and spatial distributions of total gaseous mercury concentrations in ambient air in a

476 mountainous area in southwestern China: Implications for industrial and domestic mercury
477 emissions in remote areas in China, Sci. Total. Environ., 407, 2306–2314, 2009.
478 Fu, X. W., Feng, X. B., Dong, Z. Q., Yin, R. S., Wang, J. X., Yang, Z. R., and Zhang, H.:
479 Atmospheric gaseous elemental mercury (GEM) concentrations and mercury depositions at a
480 high-altitude mountain peak in south China, Atmos. Chem. Phys., 10, 2425–2437, 2010a.
481 Fu, X. W., Feng, X. B., Zhang, G., Xu, W. H., Li, X. D., Yao, H., Liang, P., Li, J., Sommar, J., Yin,
482 R. S., and Liu, N.: Mercury in the marine boundary layer and seawater of the South China Sea:
483 concentrations, sea/air flux, and implication for land outflow, J. Geophys. Res., 115, 6303,
484 2010b.
485 Fu, X. W., Feng, X. B., Qiu, G. L., Shang, L. H., and Zhang, H.: Speicated atmospheric mercury
486 and its potential source in Guiyang, China, Atmos. Environ., 45, 4205–4212, 2011.
487 Fu, X. W., Feng, X. B., Sommar, J., and Wang, S. F.: A review of studies on atmospheric mercury
488 in China, Sci. Total. Environ., 421–422, 73–81, 2012a.
489 Fu, X. W., Feng, X. B., Shang, L. H., Wang, S. F., and Zhang, H.: Two years of measurements of
490 atmospheric total gaseous mercury (TGM) at a remote site in Mt. Changbai area, Northeastern
491 China, Atmos. Chem. Phys., 12, 4215–4226, 2012b.
492 Fu, X. W., Feng, X. B., Liang, P., Deli-Geer, Zhang, H., Ji, J., and Liu, P.: Temporal trend and
493 sources of speciated atmospheric mercury at Waliguan GAW station northwestern China, Atmos.
494 Chem. Phys., 12, 1951–1964, 2012c.
495 Gabriel, M. C., Williamson, D. G., Brooks, S., and Lindberg, S.: Atmospheric speciation of
496 mercury in two contrasting Southeastern US airsheds, Atmos. Environ., 39, 4947–4958, 2005.
497 Gustin, M. S., Lindberg, S. E., and Weisberg, P. J.: An update on the natural sources and sinks of
498 atmospheric mercury, Appl. Geochem., 23, 482–493, 2008.
499 Gustin, M. S., Huang, J.Y., Miller, M. B., Peterson, C., Jaffe, D. A., Ambrose, J., Finley, B. D.,
500 Lyman, S. N., Call, K., Talbot, R., Feddersen, D., Mao, H. T., and Lindberg, S. E.: Do we
501 understand what the mercury speciation instruments are actually measuring? Results of RAMIX,
502 Environ. Sci. Technol., 2013, doi: 10.1021/es3039104.
503 Landis, M. S., Stevens, R. K., Schaedlich, F., and Prestbo, E. M.: Development and
504 characterization of an annular denuder methodology for the measurement of divalent inorganic
505 reactive gaseous mercury in ambient air, Environ. Sci. Technol., 36, 3000–3009, 2002.

506 Laurier, F., and Mason, R.: Mercury concentration and speciation in the coastal and open ocean
507 boundary layer, J. Geophys. Res., 112, 6302, 2007.
508 Li, Z., Xia, C. H., Wang, X. M., Xia, Y. R., and Xie, Z. Q.: Total gaseous mercury in Pearl River
509 Delta region, China during 2008 winter period, Atmos. Environ., 45, 834–838, 2011.
510 Lindberg, S., Bullock, R., Ebinghaus, R., Engstrom, D., Feng, X. B., Fitzgerald, W., Pirrone, N.,
511 Prestbo, E., and Seigneur, C.: A synthesis of progress and uncertainties in attributing the sources
512 of mercury in deposition, Ambio., 36, 19–32, 2007.
513 Liu, S. L., Nadim, F., Perkins, C., Carley, R. J., Hoag, G. E., Lin, Y. H., and Chen, L. T.:
514 Atmospheric mercury monitoring survey in Beijing, China. Chemos., 48, 97–107, 2002.
515 Lynam, M., and Keeler, G. J.: Artifacts associated with the measurement of particulate mercury in
516 an urban environment: The influence of elevated ozone concentrations, Atmos. Environ., 39,
517 3081–3088, 2005.
518 Malcolm, E. G., Keeler, G. J., and Landis, M. S.: The effects of the coastal environment on the
519 atmospheric mercury cycle, J. Geophys. Res., 108, 4357, 2003.
520 Nguyen, D. L., Kim, J. Y., Shim, S. G., and Zhang, X. S.: Ground and shipboard measurements of
521 atmospheric gaseous elemental mercury over the Yellow Sea region during 2007–2008, Atmos.
522 Environ., 45, 253–260, 2011.
523 Polissar, A. V., Hopke, P. K., Paatero, P., Kaufmann, Y. J., Hall, D. K., Bodhaine, B. A., Dutton, E.
524 G., and Harris, J. M.: The aerosol at Barrow, Alaska: long-term trends and source locations,
525 Atmos. Environ., 33, 2441–2458, 1999.
526 Schroeder, W. H., and Munthe, J.: Atmospheric mercury: An overview, Atmos. Environ., 32,
527 809–822, 1998.
528 Sheu, G. R., Mason, R. P., and Lawson, N. M.: Speciation and distribution of atmospheric mercury
529 over the northern Chesapeake Bay, ACS Symp. Ser., 806, 223–242, 2002.
530 Sigler, J. M., and Lee, X.: Recent trends in anthropogenic mercury emission in the northeast
531 United States, J. Geophys. Res., 111, 14316, 2006.
532 Sprovieri, F., Pirrone, N., Ebinghaus, R., Kock, H., and Dommergue, A.: A review of worldwide
533 atmospheric mercury measurements, Atmos. Chem. Phys., 10, 8245–8265, 2010.
534 Valente, R. J., Shea, C., Lynn Humes, K., and Tanner, R. L.: Atmospheric mercury in the Great
535 Smoky Mountains compared to regional and global levels, Atmos. Environ., 41, 1861–1873,

2007.

Wan, Q., Feng, X. B., Lu, J. L., Zheng, W., Song, X. J., Han, S. J., and Xu, H.: Atmospheric mercury in Changbai Mountain area, northeastern China I: The seasonal distribution pattern of total gaseous mercury and its potential sources, Environ. Res., 109, 201–206, 2009a.

Wan, Q., Feng, X. B., Lu, J., Zheng, W., Song, X. J., Li, P., Han, S. J. and Xu, H.: Atmospheric mercury in Changbai Mountain area, northeastern China II: The distribution of reactive gaseous mercury and particulate mercury and mercury deposition fluxes, Environ. Res., 109, 721–727, 2009b.

Wang, L. T., Zhang, Q., Hao, J. M., and He, K. B.: Anthropogenic CO emission inventory of Mainland China, Acta. Scientiae. Circumstantiae., 25, 1580–1585, 2005. (in Chinese)

Wang, Y. Q., Zhang, X. Y., and Draxler, R.: TrajStat: GIS-based software that uses various trajectory statistical analysis methods to identify potential sources from long-term air pollution measurement data, Environ. Modell. Softw., 24, 938–939, 2009.

Wang, Y. X., McElroy, M. B., Munger, J. W., Hao, J. M., Ma, H., Nielsen, C. P., and Chen, Y.: Variations of O_3 and CO in summertime at a rural site near Beijing, Atmos. Chem. Phys., 8, 6355–6363, 2008.

Wang, Z. W., Chen, Z. S., Duan, N., and Zhang, X. S.: Gaseous elemental mercury concentration in atmosphere at urban and remote sites in China, J. Environ. Sci., 19, 176–180, 2007.

Weiss-Penzias, P., Jaffe, D., Swartzendruber, P., Hafner, W., Chand, D., and Prestbo, E.: Quantifying Asian and biomass burning sources of mercury using the Hg/CO ratio in pollution plumes observed at the Mount Bachelor observatory, Atmos. Environ., 41, 4366–4379, 2007.

Wu, Y., Streets, D. G., Wang, S. X., and Hao, J. M.: Uncertainties in estimating mercury emissions from coal-fired power plants in China, Atmos. Chem. Phys., 10, 2937–2946, 2010.

Wu, Y., Wang, S. X., Streets, D. G., Hao, J. M., Chan, M., and Jiang, J. K.: Trends in anthropogenic mercury emissions in China from 1995 to 2003, Environ. Sci. Technol., 40, 5312–5318, 2006.

Xu, X., and Akhtar, U. S.: Identification of potential regional sources of atmospheric total gaseous mercury in Windsor, Ontario, Canada using hybrid receptor modeling, Atmos. Chem. Phys., 10, 7073–7083, 2010.

Yang, Y. K., Chen, H., and Wang, D. Y.: Spatial and temporal distribution of gaseous elemental

mercury in Chongqing, China, Environ. Monit. Assess., 156, 479–489, 2009.

Zhang, H.: Concentrations of speciated atmospheric mercury a high-altitude background station in the Shangri-La area of Tibetan Plateau, China, Abstract to 10th international conference on Mercury as a global pollutant, Halifax, Canada, 2011.

Zhu, W. Z., Fu, X. W., Feng, X. B., and Lu, J. Y.: Annual time-series analyses of total gaseous mercury measurement and its impact factors on the Gongga Mountains in the southeastern fringe of the Qinghai-Tibetan Plateau, J. Mt. Sci., 5, 17–31, 2008.

Zhu, J., Wang, T., Talbot, R., Mao, H., Hall, C. B., Yang, X., Fu, C., Zhuang, B., Li, S., Han, Y., and Huang, X.: Characteristics of atmospheric Total Gaseous Mercury (TGM) observed in urban Nanjing, China, Atmos. Chem. Phys., 12, 12103–12118, 2012.

Tables

Table 1. Statistics of the overall monitoring data and averages in heavy pollution periods for the GEM, RGM and PBM at Miyun, Beijing

		GEM (ng/m^3)	RGM (pg/m^3)	PBM (pg/m^3)
Statistics	Mean value	3.22	10.06	98.19
	Standard deviation	1.74	18.83	112.72
	Minimum	0.39	0.12	0.49
	1st quartile	1.81	2.59	21.78
	Median (2nd quartile)	2.94	5.02	57.31
	3rd quartile	4.12	10.77	134.48
	Maximum	14.83	301.20	1090.24
Heavy pollution episodes	I: May 4th–6th, 2009	4.42	4.31	178.37
	II: August 12th–14th, 2009	3.43	10.92	50.38
	III: November 5th–7th, 2009	9.69	82.55	373.04

582 **Table 2. Summary of atmospheric speciated mercury concentrations in China**

Location	Classification	Time period	TGM (ng/m^3)	PBM (pg/m^3)	RGM (pg/m^3)	PBM/GEM (10^{-3})	RGM/GEM (10^{-3})	Reference
Guiyang	Urban	Aug 2009 – Dec 2009	9.7	368	35.7	38	3.7	Fu et al., 2011
Shanghai	Urban	Aug 2009 – Sep 2009	2.7	–	–	–	–	Friedli et al., 2011
Nanjing	Urban	Jan 2011 – Dec 2011	7.9	–	–	–	–	Zhu et al., 2012
Ningbo	Urban	Oct 2007 – Jan 2008	3.79	–	–	–	–	Nguyen et al., 2011
Chongqing	Urban	Aug 2006 – Sep 2007	6.74	–	–	–	–	Yang et al., 2009
Changchun	Urban	Jul 1999 – Jan 2000	18.4	276	–	15	–	Fang et al., 2004
Changchun	Rural	Jul 1999 – Jan 2000	11.7	109	–	9	–	Fang et al., 2004
Miyun, Beijing	Rural	Dec 2008 – Nov 2009	3.23	98.2	10.1	30	3.1	This study
Chengshantou, Weihai	Remote	Jul 2007 – May 2009	2.31	–	–	–	–	Ci et al., 2011a
Pearl River Delta	Remote	Nov 2008 – Dec 2008	2.94	–	–	–	–	Li et al., 2011
Mt. Changbai	Remote	Aug 2005 – Jul 2006	3.58	77	65	22	18.5	Wan et al., 2009a, 2009b
Mt. Changbai	Remote	Oct 2008 – Oct 2010	1.60	–	–	–	–	Fu et al., 2012b
Mt. Gongga	Remote	May 2005 – July 2007	3.98	30.7	6.2	8	1.6	Fu et al., 2008a, 2008b
Mt. Leigong	Remote	May 2008 – May 2009	2.80	–	–	–	–	Fu et al., 2010a
Mt. Waliguan	Remote	Sep 2007 – Aug 2008	1.98	19.4	7.4	10	3.8	Fu et al., 2012c
Shangri-La	Remote	Nov 2009 – Nov 2010	2.59	43.5	8.2	17	3.2	Zhang, 2011
South China Sea	Remote	Aug 2007	2.62	–	–	–	–	Fu et al., 2010b
Yellow Sea	Remote	Jul 2010	2.61	–	–	–	–	Ci et al., 2011b

583

584

585 **Table 3. Correlation coefficients between mercury species and meteorological**
586 **factors in different seasons**

Correlation	Winter	Spring	Summer	Autumn
GEM – temperature	0.21	0.35	−0.06	0.03
RGM – temperature	0.06	**0.45**	**0.46**	−0.01
PBM – temperature	0.07	−0.05	−0.20	−0.13
GEM – relative humidity	**0.47**	**0.46**	**0.48**	**0.48**
RGM – relative humidity	**0.40**	−0.04	**−0.42**	0.04
PBM – relative humidity	**0.51**	**0.44**	0.31	**0.41**

587

588

589

590 **Figure Captions**

591 **Fig. 1. The location of the Miyun monitoring station in Beijing, China.**

592 **Fig. 2. Hourly averaged GEM, RGM and PBM concentrations at monitoring site**
593 **and air pollution index (API) in Beijing urban area from December 2008 to**
594 **November 2009.**

595 **Fig. 3. Monthly variation of (a) GEM and seasonal variation of (b) RGM and (c)**
596 **PBM concentration.**

597 **Fig. 4. Daily variation of (a) GEM, (b) RGM and (c) PBM concentration.**

598 **Fig. 5. Statistics of (a) average GEM concentration, (b) average RGM**
599 **concentration, (c) average PBM concentration and (d) wind direction frequency**
600 **in different wind directions.**

601 **Fig. 6. Correlation between CO concentration and GEM concentration.**

602 **Fig. 7. Comparison of O_3 and RGM concentrations in different seasons.**

603 **Fig. 8. Relationship between RGM/O_3 ratio and O_3-RGM correlation coefficient.**

604 **Fig. 9. Relationship between $PM_{2.5}$ and PBM in different seasons.**

605 **Fig. 10. HYSPLIT modeling results for the period of (a) May 4–6, (b) August**
606 **12–14, and (c) November 5–7, 2009.**

607 **Fig. 11. Spatial contribution of mercury emission sources simulated by PSCF**
608 **model (a: overall; b: winter; c: spring; d: summer; e: autumn).**

609

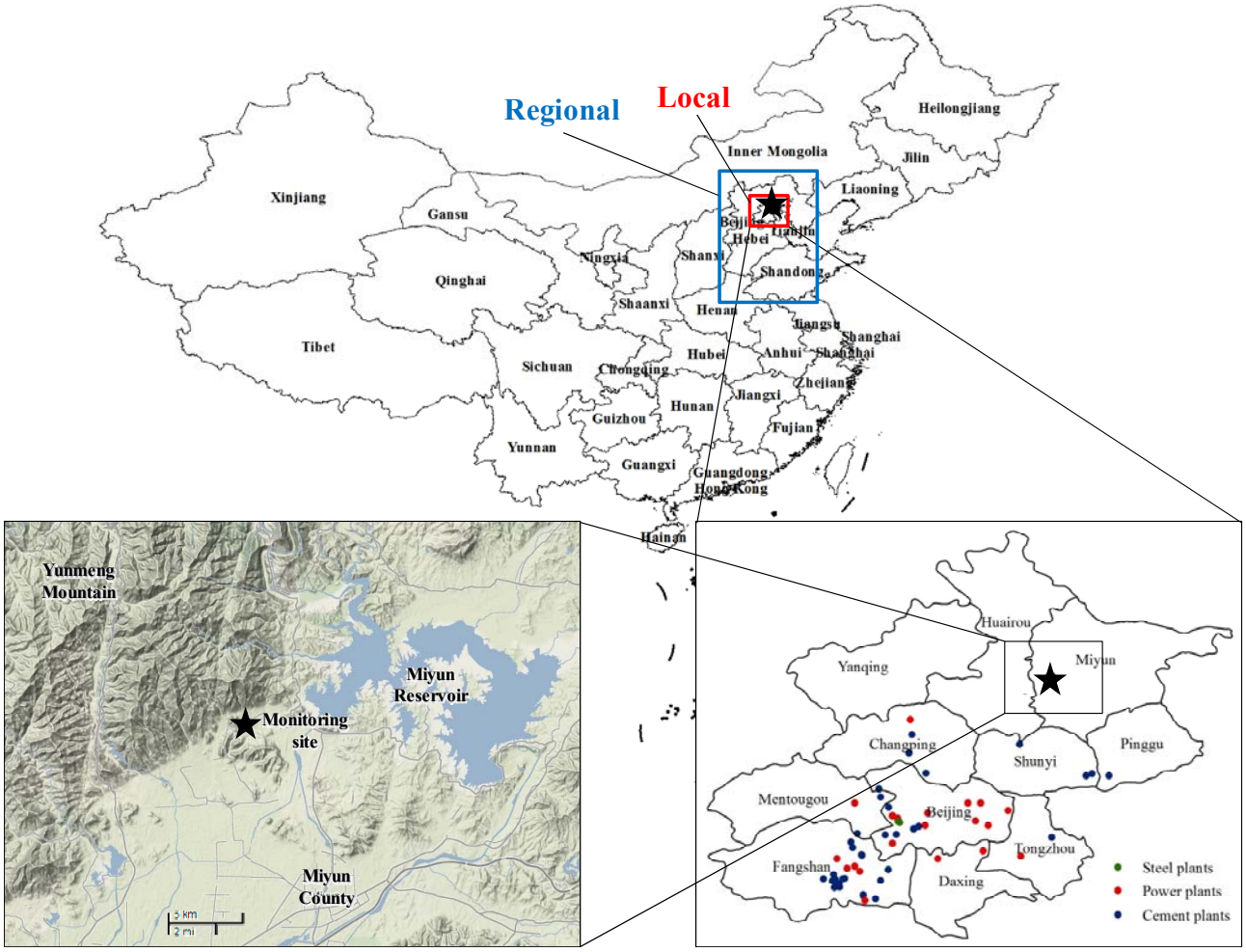

Fig. 1. The location of the Miyun monitoring station in Beijing, China.

Notes: Large point sources include power plants, cement plants, and iron and steel plants. Large power plants are defined as those whose installed capacities are larger than 6 MW. Large cement plants are defined as those whose production capacities of cement are larger than 15 kt/yr. Large iron and steel plants are defined as those whose production capacities of crude steel are larger than 1000 kt/yr.

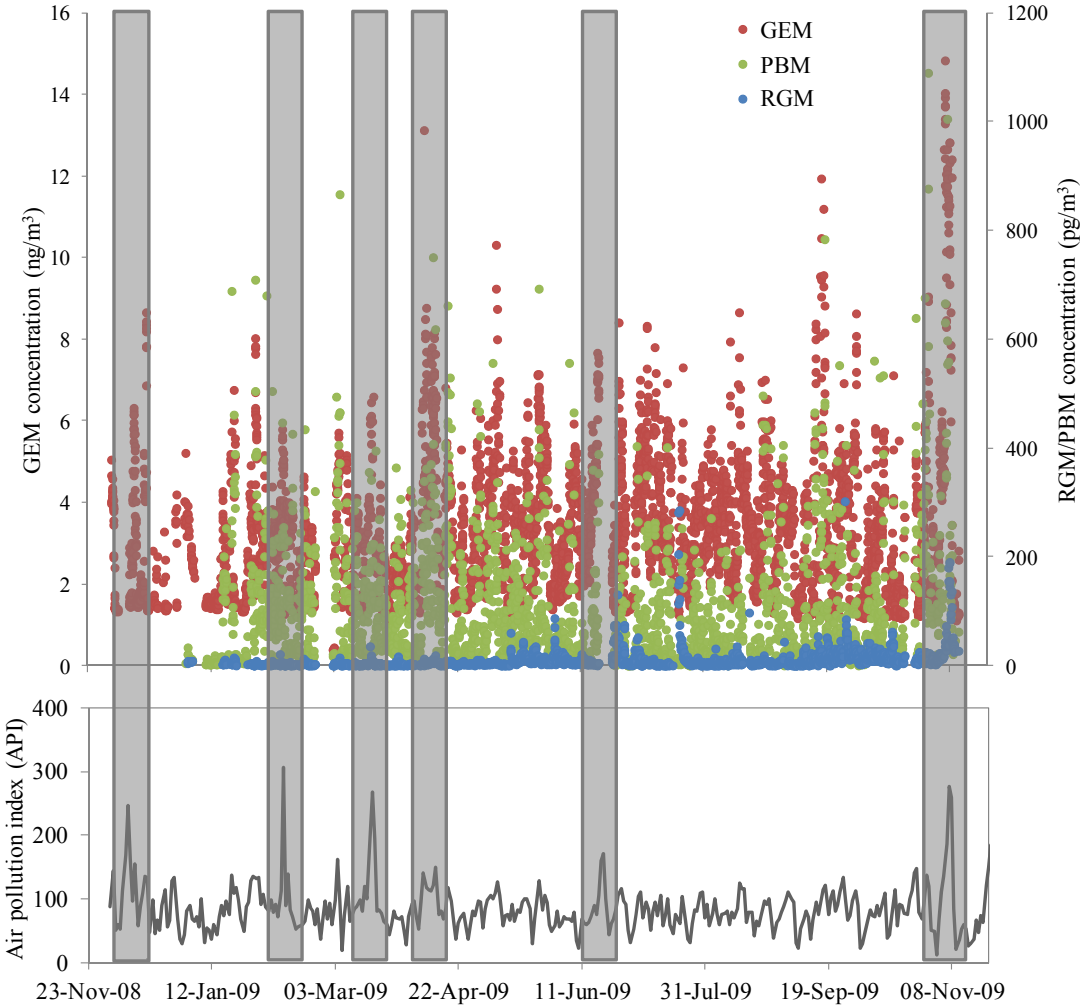

617

618 **Fig. 2. Hourly averaged GEM, RGM and PBM concentrations at monitoring site**
619 **and air pollution index (API) in Beijing urban area from December 2008 to**
620 **November 2009.**

621 Notes: The six grey columns are typical heavy pollution episodes in Beijing urban area.

622

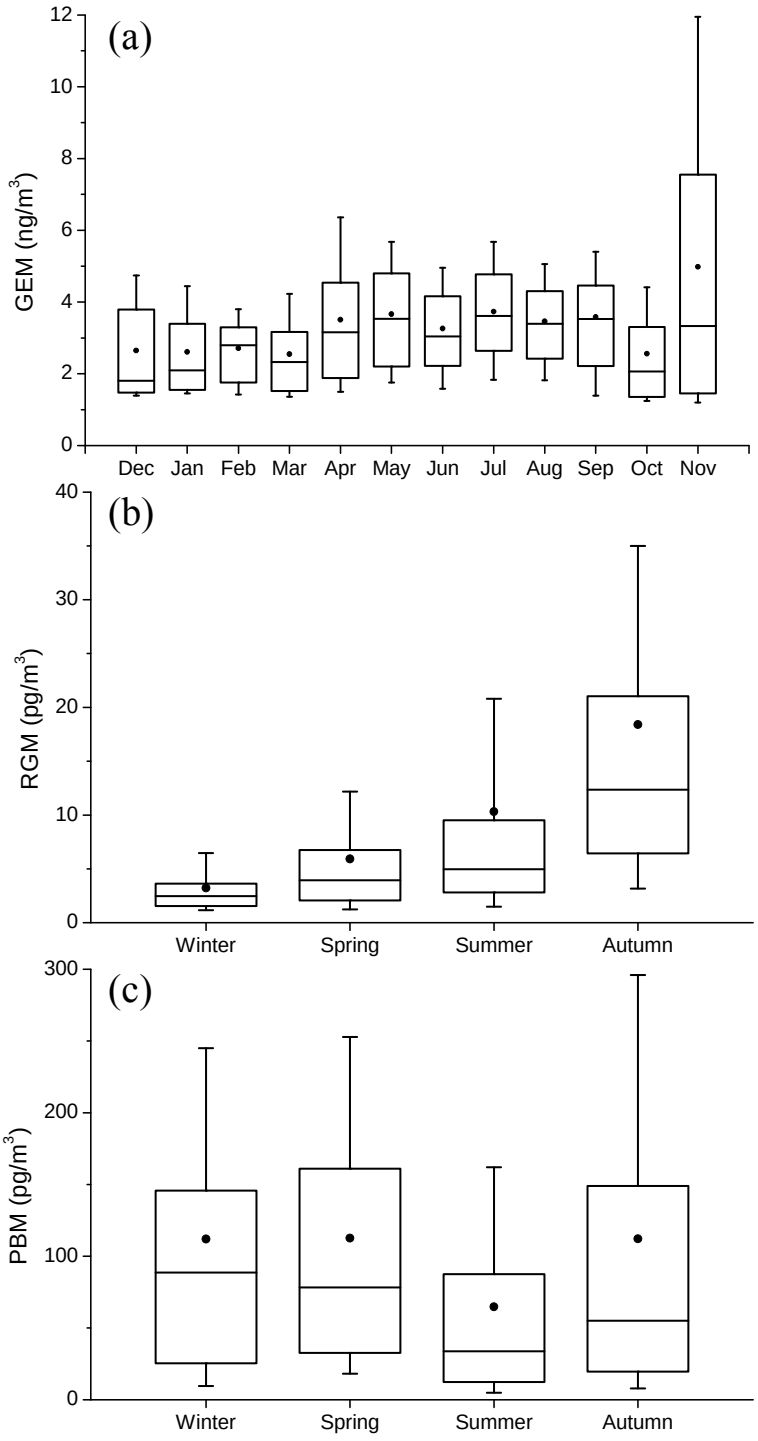

623

624 **Fig. 3. Monthly variation of (a) GEM and seasonal variation of (b) RGM and (c)**
625 **PBM concentration.**

626 Notes: The bottom and top of the box represent the 25th and 75th percentiles (the lower and upper
627 quartiles), respectively. The band near the middle of the box represents the 50th percentile (the
628 median). The ends of the whiskers represent the 10th and 90th percentiles. The dots represent the
629 mean values.

630

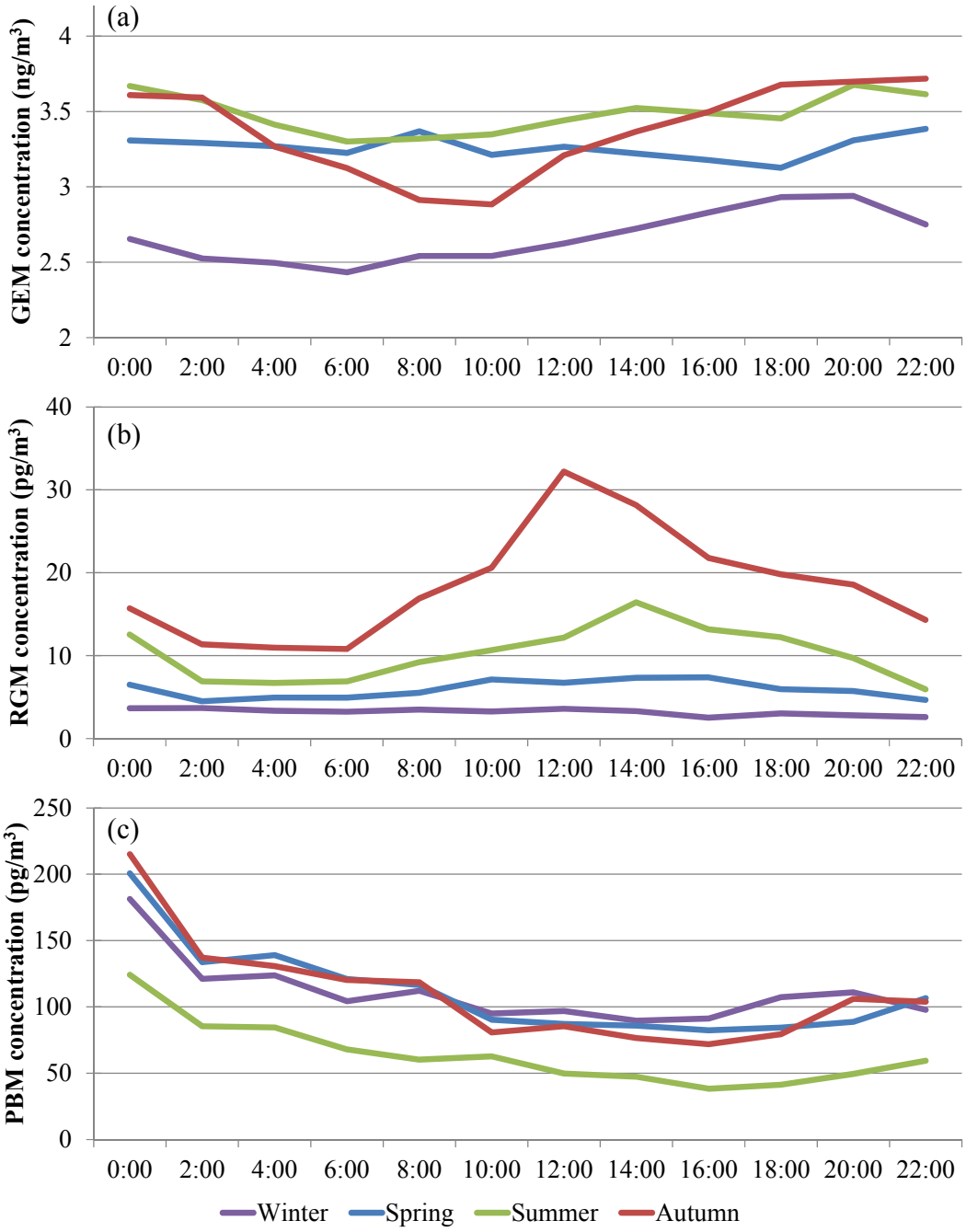

631

632 **Fig. 4. Daily variation of (a) GEM, (b) RGM and (c) PBM concentration.**

633 Notes: The data was two hourly averaged.

634

635

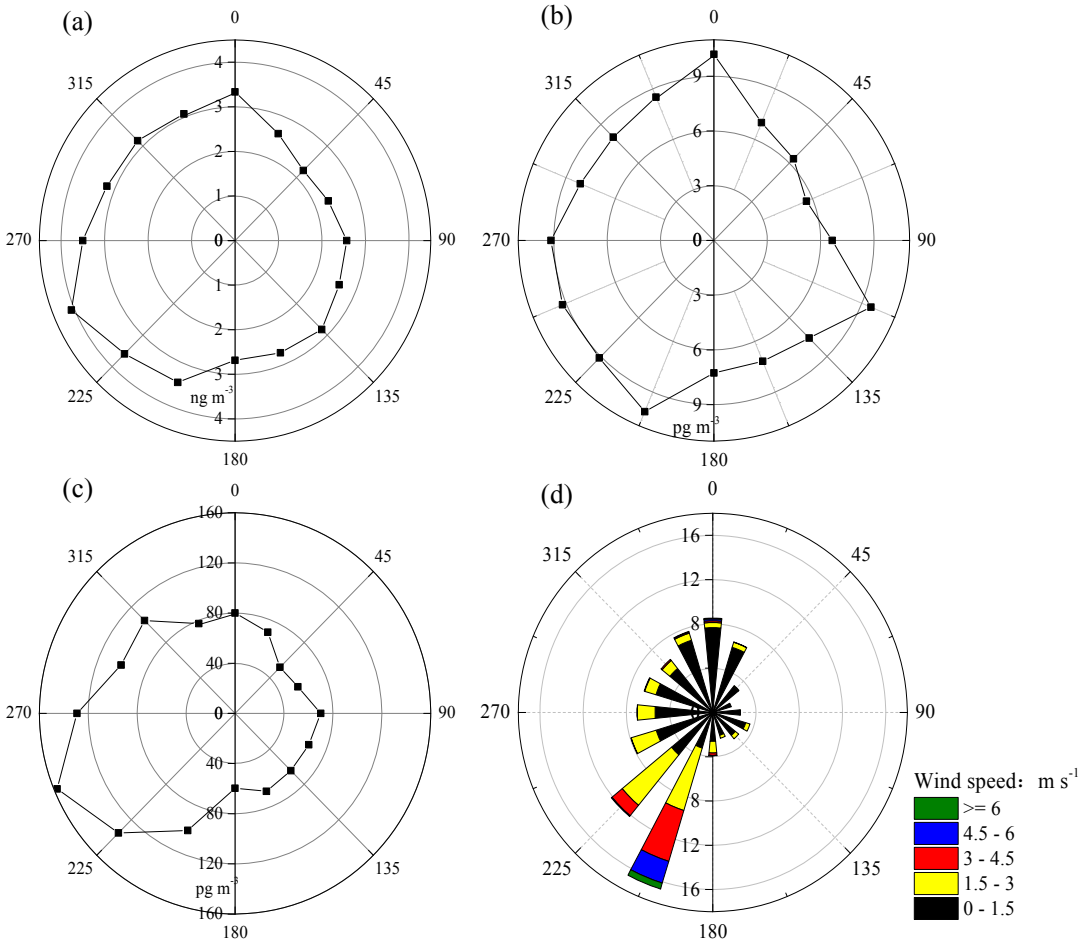

636

637 **Fig. 5. Statistics of (a) average GEM concentration, (b) average RGM**
638 **concentration, (c) average PBM concentration and (d) wind direction frequency**
639 **in different wind directions.**

640

641

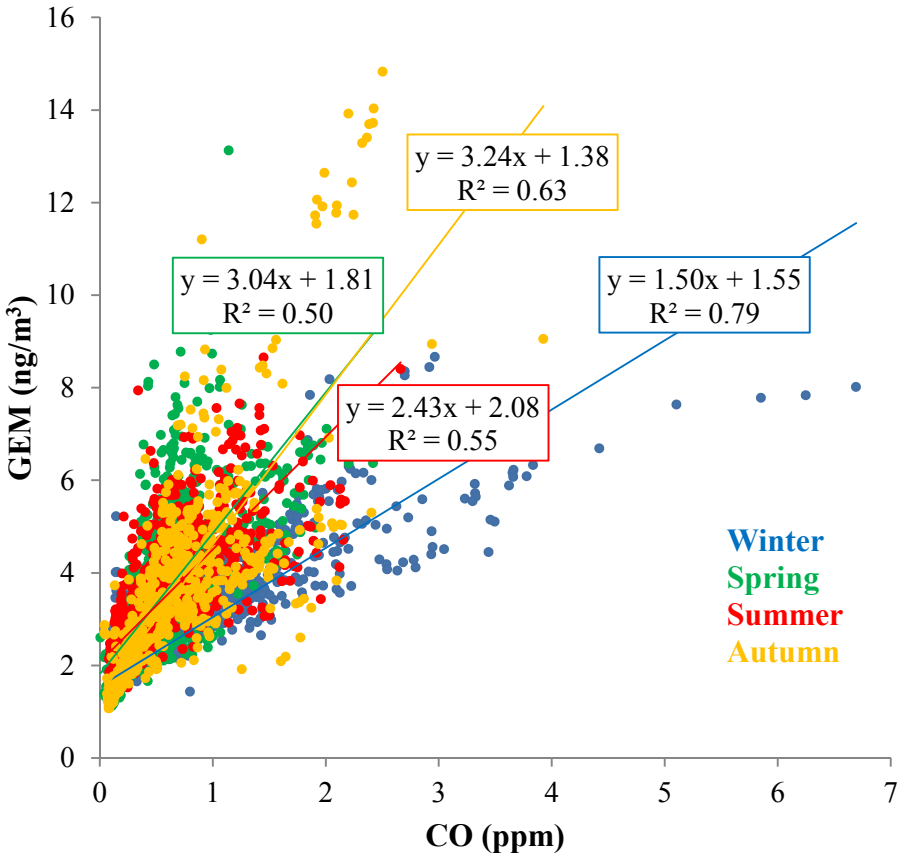

642

643 **Fig. 6. Correlation between CO concentration and GEM concentration.**

644 Notes: The data was hourly averaged.

645

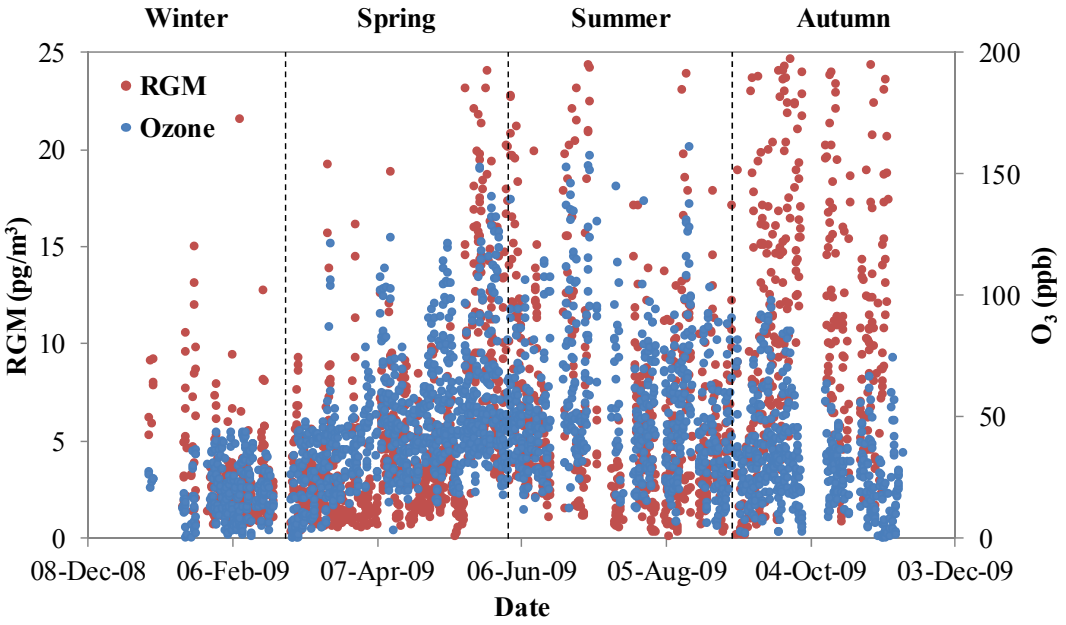

Fig. 7. Comparison of O_3 and RGM concentrations in different seasons.

Notes: The data was hourly averaged.

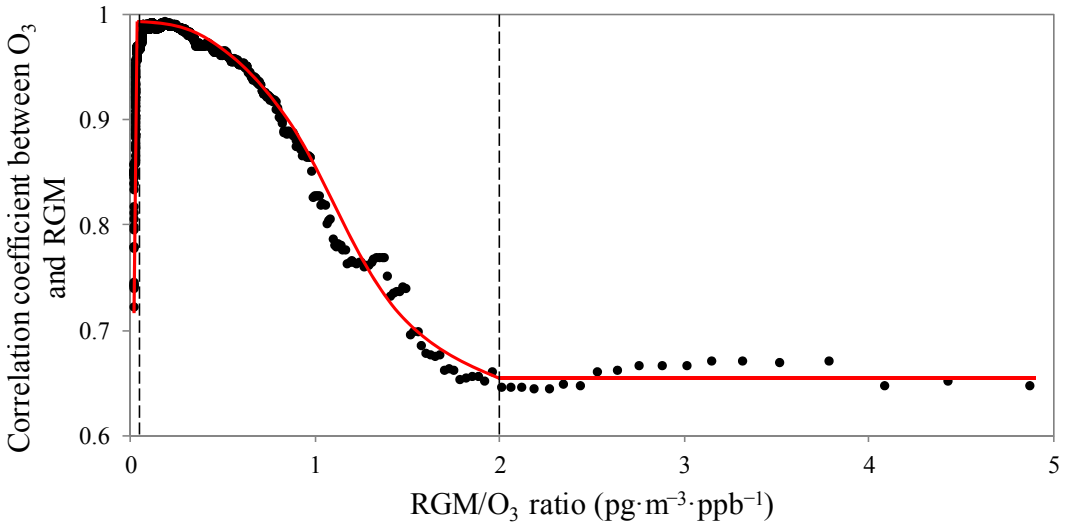

Fig. 8. Relationship between RGM/O_3 ratio and O_3-RGM correlation coefficient.

Notes: The data was hourly averaged.

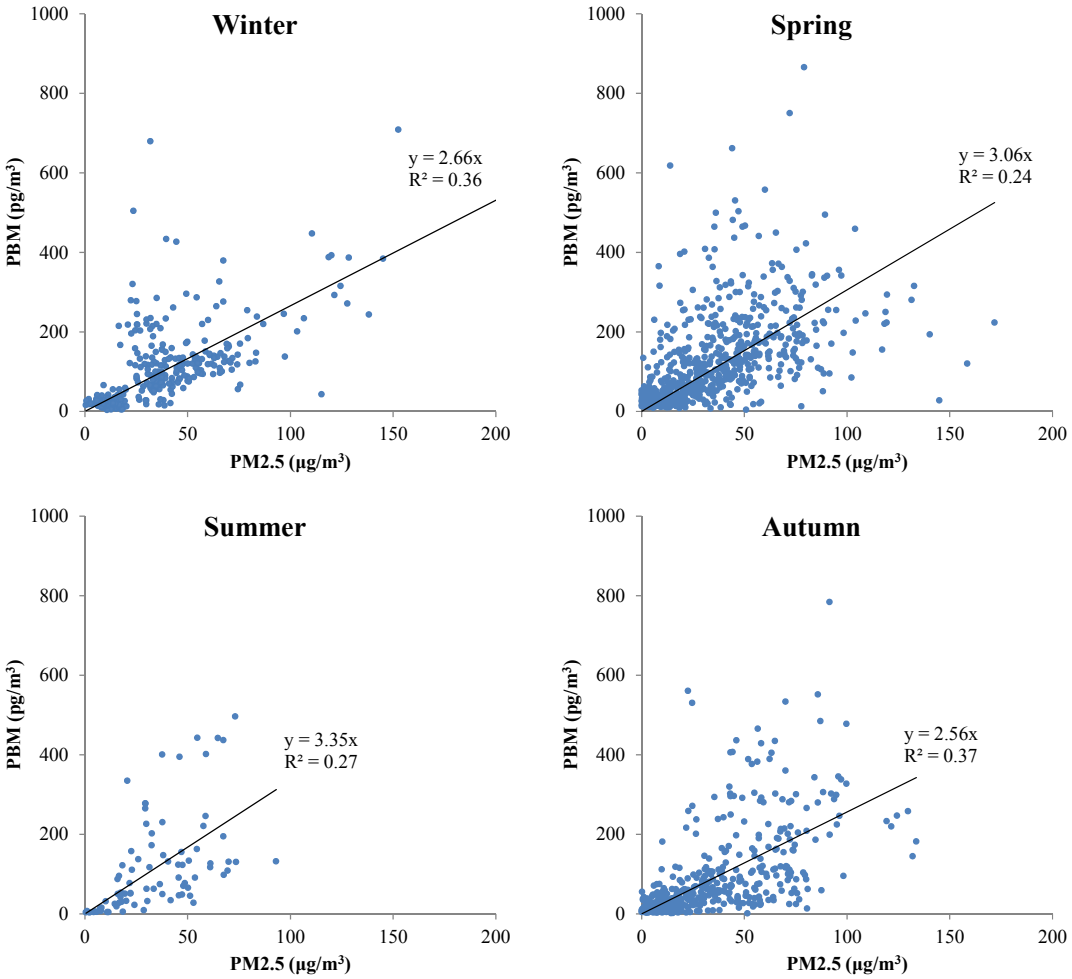

Fig. 9. Relationship between $PM_{2.5}$ and PBM in different seasons.

Notes: The data was hourly averaged.

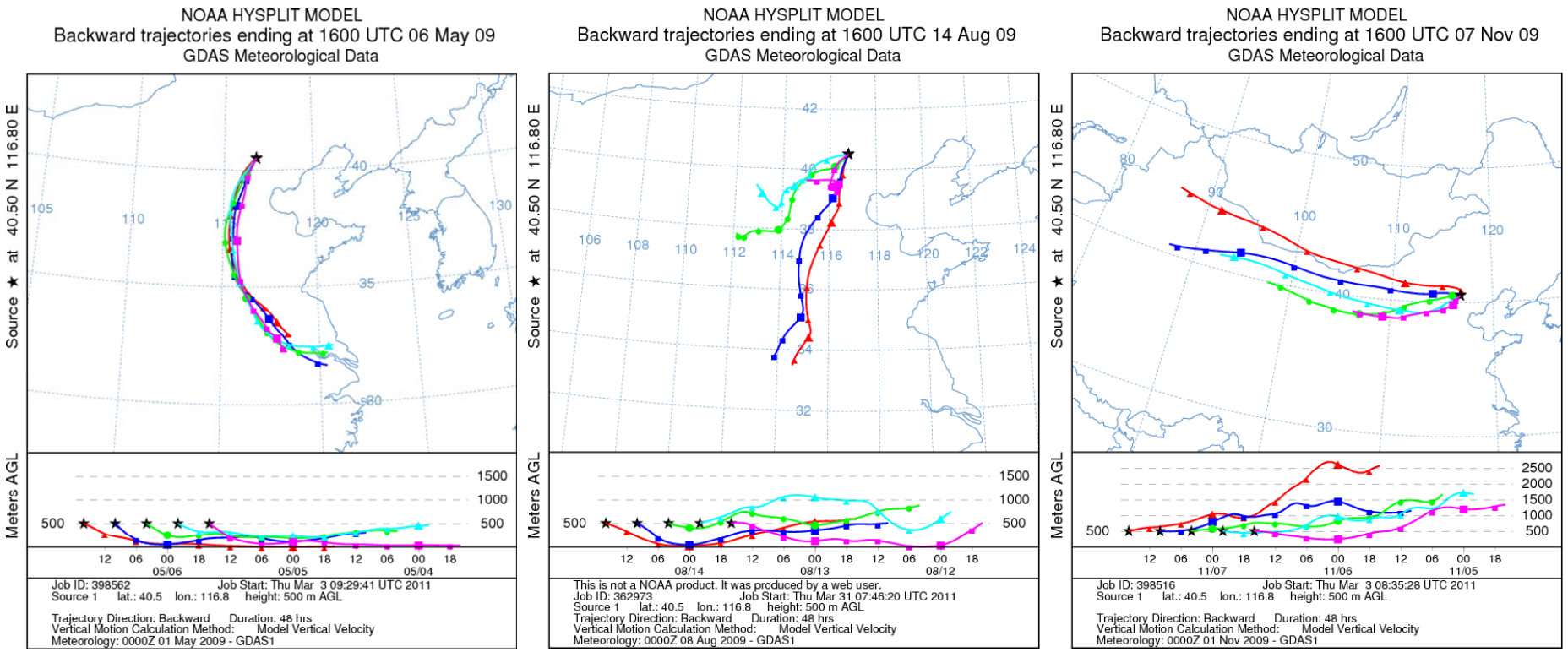

(a) (b) (c)

Fig. 10. HYSPLIT modeling results for the period of (a) May 4–6, (b) August 12–14, and (c) November 5–7, 2009.

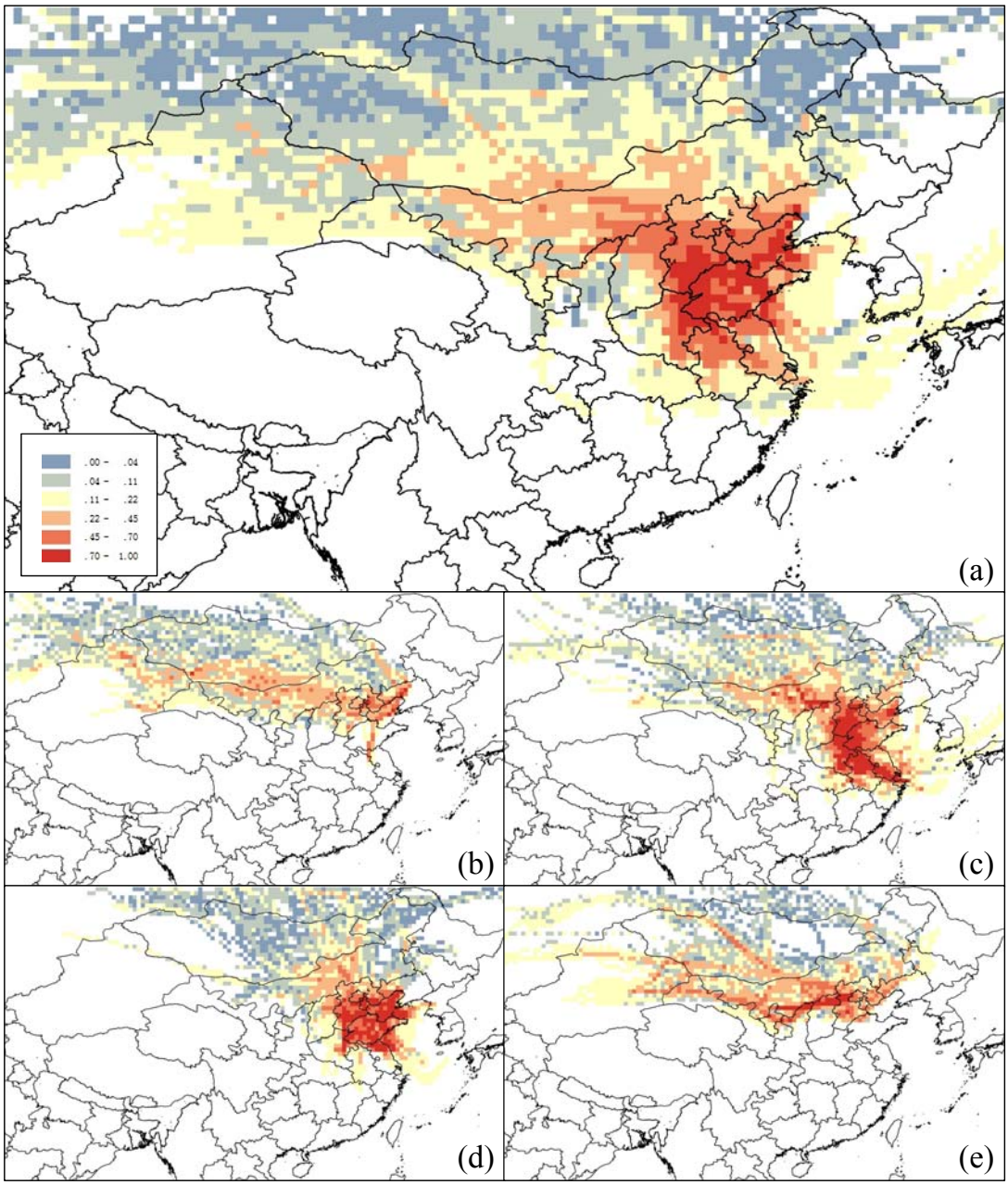

Fig. 11. Spatial contribution of mercury emission sources simulated by PSCF model (a: overall; b: winter; c: spring; d: summer; e: autumn).